

Multiple surface states, nontrivial band topology, and antiferromagnetism in $GdAuAl_4Ge_2$

Chengcheng Zhang(张成成), Yuan Wang(王渊), Fayuan Zhang(张发远), Hongtao Rong(戎洪涛), Yongqing Cai(蔡永青), Le Wang(王乐), Xiao-Ming Ma(马小明), Shu Guo(郭抒), Zhongjia Chen(陈仲佳), Yanan Wang(王亚南), Zhicheng Jiang(江志诚), Yichen Yang(杨逸尘), Zhengtai Liu(刘正太), Mao Ye(叶茂), Junhao Lin(林君浩), Jiawei Mei(梅佳伟), Zhanyang Hao(郝占阳), Zijuan Xie(谢子娟), and Chaoyu Chen(陈朝宇)
Citation: Chin. Phys. B, 2023, 32 (**7**): 077401. DOI: 10.1088/1674-1056/acca0e
Journal homepage: http://cpb.iphy.ac.cn; http://iopscience.iop.org/cpb

What follows is a list of articles you may be interested in

Superconductivity and unconventional density waves in vanadium-based kagome materials AV_3Sb_5

Hui Chen(陈辉), Bin Hu(胡彬), Yuhan Ye(耶郁晗), Haitao Yang(杨海涛), and Hong-Jun Gao(高鸿钧)
Chin. Phys. B, 2022, 31 (**9**): 097405. DOI: 10.1088/1674-1056/ac7f95

Surface-induced orbital-selective band reconstruction in kagome superconductor CsV_3Sb_5

Linwei Huai(淮琳崴), Yang Luo(罗洋), Samuel M. L. Teicher, Brenden R. Ortiz, Kaize Wang(王铠泽),Shuting Peng(彭舒婷), Zhiyuan Wei(魏志远), Jianchang Shen(沈建昌), Bingqian Wang(王冰倩), Yu Miao(缪宇),Xiupeng Sun(孙秀鹏), Zhipeng Ou(欧志鹏), Stephen D. Wilson, and Junfeng He(何俊峰)
Chin. Phys. B, 2022, 31 (**5**): 057403. DOI: 10.1088/1674-1056/ac4f50

Dispersion of neutron spin resonance mode in $Ba_{0.67}K_{0.33}Fe_2As_2$

Tao Xie(谢涛), Chang Liu(刘畅), Tom Fennell, Uwe Stuhr, Shi-Liang Li(李世亮), and Hui-Qian Luo(罗会仟)
Chin. Phys. B, 2021, 30 (**12**): 127402. DOI: 10.1088/1674-1056/ac3651

Surface Majorana flat bands in j=3/2 superconductors with singlet-quintet mixing

Jiabin Yu(于家斌), Chao-Xing Liu(刘朝星)
Chin. Phys. B, 2020, 29 (**1**): 017402. DOI: 10.1088/1674-1056/ab5b89

Topological superconductivity in a $Bi_2Te_3/NbSe_2$ heterostructure: A review

Hao Zheng(郑浩), Jin-Feng Jia(贾金锋)
Chin. Phys. B, 2019, 28 (**6**): 067403. DOI: 10.1088/1674-1056/28/6/067403

Multiple surface states, nontrivial band topology, and antiferromagnetism in $GdAuAl_4Ge_2$

Chengcheng Zhang(张成成)[1], Yuan Wang(王渊)[1], Fayuan Zhang(张发远)[1], Hongtao Rong(戎洪涛)[1], Yongqing Cai(蔡永青)[1], Le Wang(王乐)[1], Xiao-Ming Ma(马小明)[1], Shu Guo(郭抒)[1], Zhongjia Chen(陈仲佳)[2,3], Yanan Wang(王亚南)[2,3], Zhicheng Jiang(江志诚)[4], Yichen Yang(杨逸尘)[4], Zhengtai Liu(刘正太)[4], Mao Ye(叶茂)[4], Junhao Lin(林君浩)[1], Jiawei Mei(梅佳伟)[1], Zhanyang Hao(郝占阳)[1,†], Zijuan Xie(谢子娟)[5,‡], and Chaoyu Chen(陈朝宇)[1,§]

[1] *Shenzhen Institute for Quantum Science and Engineering (SIQSE) and Department of Physics, Southern University of Science and Technology (SUSTech), Shenzhen* 518055, *China*
[2] *Songshan Lake Materials Laboratory, Dongguan* 523000, *China*
[3] *Beijing National Laboratory for Condensed Matter Physics and Institute of Physics, Chinese Academy of Sciences, Beijing* 100190, *China*
[4] *State Key Laboratory of Functional Materials for Informatics and Center for Excellence in Superconducting Electronics, Shanghai Institute of Microsystem and Information Technology, Chinese Academy of Sciences, Shanghai* 200050, *China*
[5] *International School of Microelectronics, Dongguan University of Technology, Dongguan* 523000, *China*

(Received 23 March 2023; revised manuscript received 4 April 2023; accepted manuscript online 4 April 2023)

Magnetic topological states of matter provide a fertile playground for emerging topological physics and phenomena. The current main focus is on materials whose magnetism stems from 3d magnetic transition elements, *e.g.*, $MnBi_2Te_4$, Fe_3Sn_2, and $Co_3Sn_2S_2$. In contrast, topological materials with the magnetism from rare earth elements remain largely unexplored. Here we report rare earth antiferromagnet $GdAuAl_4Ge_2$ as a candidate magnetic topological metal. Angle resolved photoemission spectroscopy (ARPES) and first-principles calculations have revealed multiple bulk bands crossing the Fermi level and pairs of low energy surface states. According to the parity and Wannier charge center analyses, these bulk bands possess nontrivial Z_2 topology, establishing a strong topological insulator state in the nonmagnetic phase. Furthermore, the surface band pairs exhibit strong termination dependence which provides insight into their origin. Our results suggest $GdAuAl_4Ge_2$ as a rare earth platform to explore the interplay between band topology, magnetism and f electron correlation, calling for further study targeting on its magnetic structure, magnetic topology state, transport behavior, and microscopic properties.

Keywords: magnetic topological material, surface state, ARPES, topological invariant

PACS: 74.25.Jb, 71.20.–b, 71.18.+y, 73.20.At **DOI:** 10.1088/1674-1056/acca0e

1. Introduction

The integration of band topology and magnetism in quantum materials gives rise to novel states of matter such as Chern insulator, axion insulator, topological Möbius insulator, Weyl semimetal, *etc.*[1–5] Such states usually host an enhanced Berry curvature and surface/edge/hinge/corner states due to the bulk–boundary correspondence, manifesting extreme responses to external stimuli such as electric/magntic field, temperature gradient and optical excitation, *e.g.*, (quantum) anomalous Hall effect, anomalous Nernst effect, topological magneto–optical effect, and negative magnetoresistance as signature of chiral anomaly. Functionalization of these effects may boost industrial development in dissipationless spintronics, information storage and quantum computation.[6–18] As a current example, $(MnBi_2Te_4)\cdot(Bi_2Te_3)_n$ ($n = 0, 1, 2, 3$) family of materials has intrigued the community as the first realization of intrinsic magnetic topological insulator.[3,4,19–24] Its lattice structure, magnetic configuration, and electronic structure possess fertile tunability,[25] which enables the realization of novel phenomena such as magnetic gap opening of topological Dirac surface state,[26] layer Hall effect,[27] Chern insulator, and axion insulator phases.[28–31] The second example is the T_3Sn_X (T = Fe, Mn; $X = 1, 2, 3$) compounds in which magnetic transition metal Fe or Mn atoms form kagome layers. The band topology inherited from the kagome layer and the multiple types of magnetic orders leads to gapped/gapless Dirac cones,[32,33] Weyl points,[34] anomalous Hall effect,[33,35] anomalous Nernst effect,[36] *etc.* These topological phenomena have also been observed in other magnetic topological materials such as $Co_3Sn_2S_2$,[37,38] Co_2MnGa,[39,40] and RMn_6Sn_6 (R = rare earth metal).[41–49] In fact, exploring new topological states and novel phenomena based on 3d magnetic transition metal atoms (Mn, Fe, Co, Ni) represents a main trend. By comparison, magnetic topological states of matter based on magnetic rare earth atoms remain largely unexplored.

†Corresponding author. E-mail: 11849277@mail.sustech.edu.cn
‡Corresponding author. E-mail: zjxie@dgut.edu.cn
§Corresponding author. E-mail: chency@sustech.edu.cn

© 2023 Chinese Physical Society and IOP Publishing Ltd

In this paper, we systematically study the magnetism, electronic structure and band topology of a newly discovered metallic antiferromagnet $GdAuAl_4Ge_2$, in which rare earth magnetic Gd^{3+} ions form a layered triangular lattice. Magnetic property measurements have revealed multiple antiferromagnetic transitions below $T_N = 17.8$ K. Angle resolved photoemission spectroscopy (ARPES) measurements and density functional theory (DFT) calculations have revealed multiple bulk bands crossing the Fermi level, which possess nontrivial Z_2 topology according to our parity and Wannier charge center analyses, establishing a strong topological insulator state in its paramagnetic phase. Furthermore, multiple pairs of low energy surface states residing in the bulk gap have been observed by ARPES. Our termination dependent surface spectra calculations exhibit acceptable agreement with the ARPES spectra, providing insight into their atomic layer origin. Our results establish rare earth antiferromagnet $GdAuAl_4Ge_2$ as a new material platform and call for further magnetic, electronic and transport studies to investigate the interplay between band topology and magnetism.

2. Methods

Single crystals of $GdAuAl_4Ge_2$ were grown by the self-flux method.[50–52] High purity Gd (block), Au (powder), Al (rod), and Ge (lump) were mixed with a ratio of 1:1:10:5 in the glovebox and placed into an alumina crucible. The crucible was then sealed into an evacuated quartz tube under vacuum to avoid oxidization during the reaction. In the furnace, the quartz tube was heated up to 1000 °C and kept at this temperature for 12 hours. Then the temperature was slowly decreased down to 700 °C in 100 hours. After the heating procedure, the quartz tube was taken into the centrifuge quickly to remove excess flux. A large number of millimeter-size single crystals were obtained.

The structure of the crystals was determined by x-ray diffraction with Cu K_α radiation at room temperature using a Rigaku MiniFlex diffractometer. Temperature and magnetic field-dependent magnetization measurements were performed for temperature $T = 2$ K–300 K and magnetic field $\mu_0 H = 0$ T–7 T applied in *ab* plane and along *c* axis using magnetic property measurement system (MPMS3, Quantum Design).

ARPES measurements were performed at the BL03U beamline of the Shanghai Synchrotron Radiation Facility with a DA30 electron analyser. The energy and angular resolution were set to be better than 10 meV and less than 0.05°, respectively. Samples were cleaved *in situ* with pressure better than 5×10^{-11} mbar (1 bar = 10^5 Pa) and temperatures below 20 K.

First-principles calculations are carried out within the framework of density functional theory (DFT)[53,54] by using the Vienna *ab-initio* Simulation Package (VASP).[55] The planewave-basis cutoff energy of 500 eV is used. The first Brillouin zone (BZ) is sampled by a $5 \times 5 \times 5$ *k*-mesh-grid.[56] We employ GGA + *U* method[57] by choosing the on-site Coulomb repulsion of $U = 4$ eV for the Au element. The f-electrons are treated as core states for the Gd element. The spin–orbit coupling effect is taken into consideration. The maximally localized Wannier functions (MLWFs) of Gd-p/d, Au-s/p/d, Al-s/p/d, and Ge-s/p ortitals are selected to construst the tight-binding model as implemented in the Wannier90 package.[58,59]

3. Results

Single crystals of $GdAuAl_4Ge_2$ adapt a rhombohedral space group $R\bar{3}m$ (No. 166) with lattice parameters $a = 4.2123(6)$ Å and $c = 30.994(6)$ Å. The crystal structure of $GdAuAl_4Ge_2$ is shown in Fig. 1(a) where Gd atoms form a triangular lattice in *ab*-plane. The unit cell is generally composed of staggered layers of Gd–Ge octahedra and Au-Al polyhedral along *c* axis. Powder x-ray diffraction is used to determine the crystal structure, as shown in Fig. 1(b), the main phase is consistent with the simulation results of $GdAuAl_4Ge_2$, and peaks of impurities introduced by the flux are marked with asterisks.[50,51]

Temperature-dependent magnetic susceptibility of $GdAuAl_4Ge_2$ is shown in Fig. 1(c). For $\mu_0 H = 0.5$ T, the magnetic susceptibility curves for the field applied in and out of the *ab*-plane coincide at the high-temperature region. No splitting is observed with the decreasing of temperature for both zero-field-cooling (ZFC) and field-cooling (FC) measurements. At low temperature, the magnetic susceptibility behaves differently for $H \parallel ab$ and $H \parallel c$, indicating the existence of magnetic anisotropy. As highlighted in Fig. 1(d), for $H \parallel ab$, there are three phase transition anomalies occurring at $T_{N1} = 17.8$ K, $T_{N2} = 15.6$ K, and $T_{N3} = 13.8$ K. Whereas only T_{N1} and T_{N3} can be observed for $H \parallel c$. For $H \parallel ab$, the magnitude of χ begins to decline below T_{N1} at $\mu_0 H = 0.5$ T. With the increase of magnetic field, the magnetic phase transitions are gradually suppressed and tend to saturate for $\mu_0 H > 1.5$ T as shown in Fig. 1(e). Similar magnetic behaviors can also be seen for $H \parallel c$ (Fig. 1(f)). The field dependence of magnetization curves at various temperatures for $H \parallel ab$ are presented in Fig. 1(g). At $T = 1.8$ K, magnetization starts out as a linear increase and subsequently undergoes an apparent upturn at $H_{C1} \sim 1.9$ T, which is considered as a spin flop transition. Then magnetization continues to increase linearly without sign of saturation up to 7 T. With increasing temperature, the transitions moves to lower fields and disappears above 15 K. For $H \parallel c$, magnetization exhibits linear behavior and no phase transition is observed. The magnetic behaviors of $GdAuAl_4Ge_2$ agree with recent work which reported it as a reservoir for complex magnetism and electronic behaviors such as the topological Hall effect.[51] Therefore, here we are prompted to focus on the electronic structure to directly unveil its topological property, leaving it unclear what is the detailed magnetic configuration.

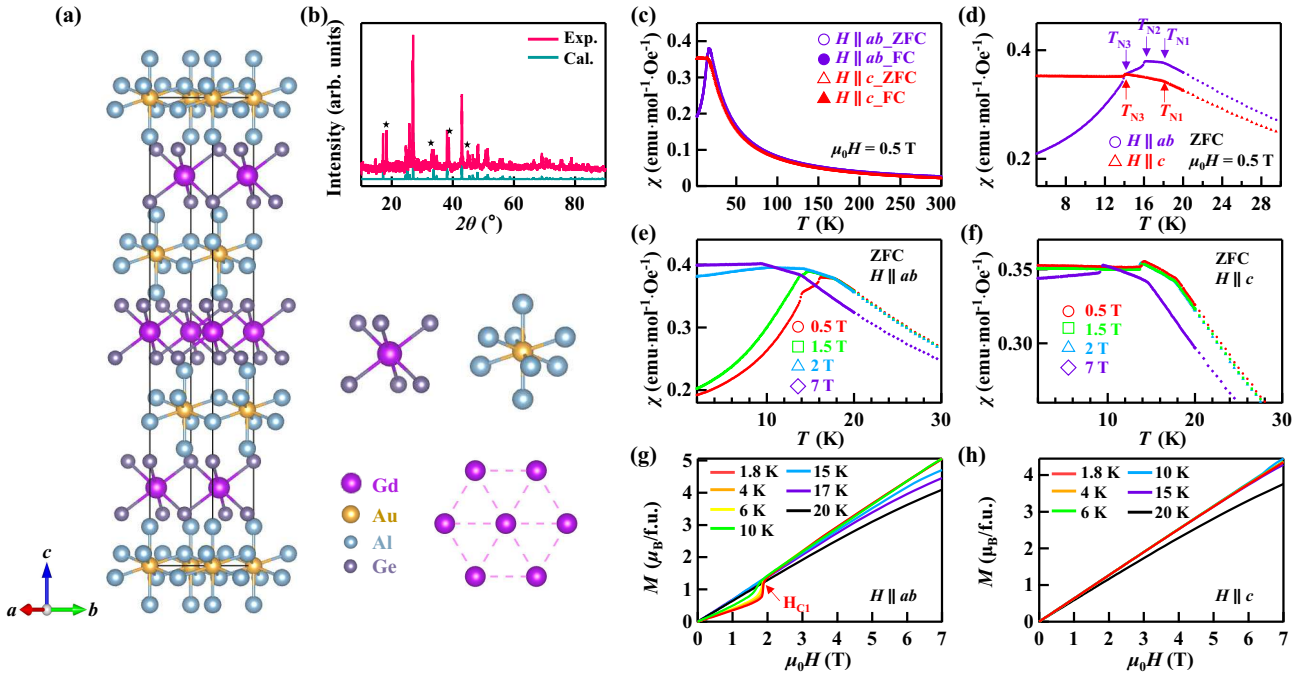


Fig. 1. Crystal structure and characterization of single-crystalline $GdAuAl_4Ge_2$. (a) Crystal structure of $GdAuAl_4Ge_2$. The local atomic arrangement of Gd–Ge and Au–Al and the triangular configuration of the Gd atomic plane are present in the right bottom. (b) Powder x-ray diffraction data for $GdAuAl_4Ge_2$. Simulated pattern is plotted in light blue for comparison and the peaks of impurities are marked with asterisks. (c) Temperature-dependent magnetic susceptibility measurements with ZFC and FC modes at $\mu_0 H = 0.5$ T for $H \parallel ab$ and $H \parallel c$ respectively. (d) Expanded view of panel (c). (e)–(f) Temperature-dependent magnetic susceptibility at different fields for $H \parallel ab$ and $H \parallel c$ respectively. (g)–(h) Field-dependent magnetization at different temperatures with fields applied in ab-plane and along c axis, respectively. The unit 1 Oe = 79.5775 A·m^{-1}.

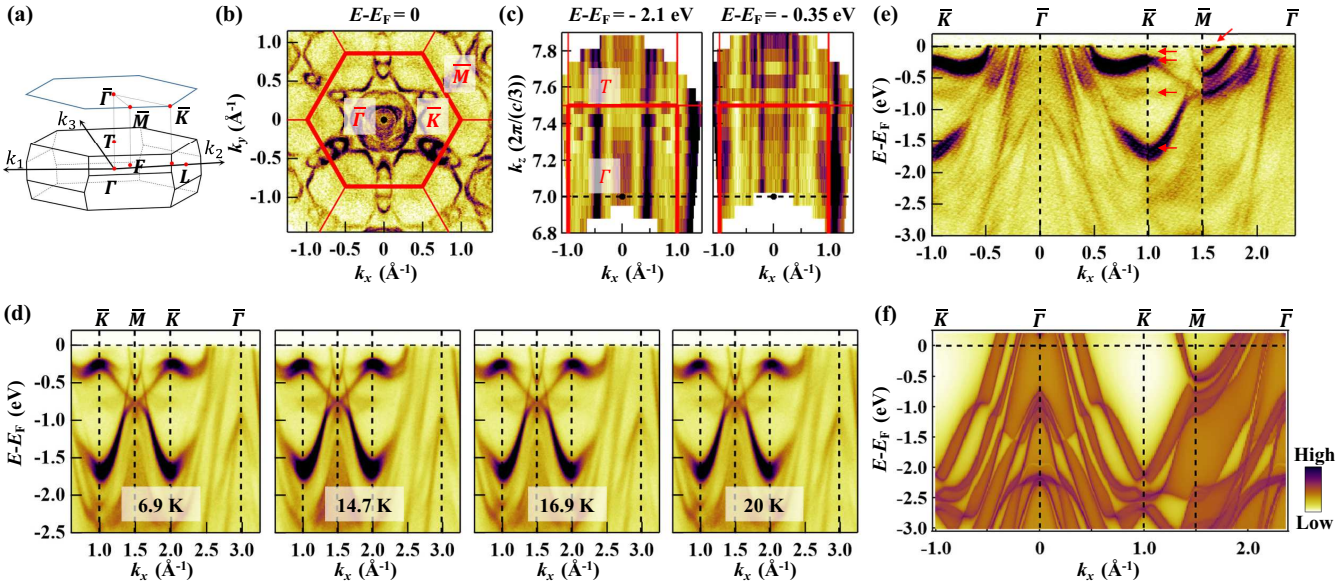


Fig. 2. Electronic structure of $GdAuAl_4Ge_2$. (a) The three-dimensional Brillouin zone (BZ) of bulk $GdAuAl_4Ge_2$ and the projected BZ for the ARPES measured (00l) surface with high symmetry points specified. (b) Fermi surface mapping on the (00l) surface using incident photons of 120 eV. The two-dimensional (2D) BZ is represented by the red lines. (c) Photon energy-dependent ARPES from 60 eV to 80 eV (k_z mapping) at $E - E_F = -2.1$ eV (left) and -0.35 eV (right) respectively, with inner potential $V_0 = 14$ eV. The 2D BZ boundary is traced in red. (d) Spectra taken along high-symmetry path $\overline{K}$–$\overline{M}$–$\overline{K}$–$\overline{\Gamma}$ at variable temperatures. (e)–(f) ARPES measured spectra and DFT calculated bulk bands along high symmetry directions.

To uncover the topological properties of $GdAuAl_4Ge_2$, we combine ARPES measurement and DFT calculations to systematically explore its electronic structure. ARPES measurements were carried out on the cleaved (00l) surface (ab plane). Figure 2(b) shows the Fermi surface mapped using photon energy of 120 eV. A hexagram-like Fermi surface can be clearly identified. The hexagonal pockets surrounding the $\overline{\Gamma}$ point and the elliptical pockets centered at the $\overline{M}$ points can be clearly distinguished. Photon energy dependent ARPES from 60 eV to 80 eV are utilized to clarify its k_z dispersion, as shown in Fig. 2(c). One can slightly identify the k_z dependent shadow features around $k_x = 0$ in the left panel. It is noted that it has a period of $2\pi/(c/3)$ rather than $2\pi/c$, which is related to the smallest repeating unit of crystal struc-

ture along c axis. Except for this, other energy bands, especially these within 2 eV below the Fermi level, have no observable k_z dispersion, in line with the layered lattice. Referring to the magnetic phase transitions in $GdAuAl_4Ge_2$, ARPES measurements were carried out at four different temperatures. As shown in Fig. 2(d), ARPES spectra show no noticeable temperature dependence, similar to some reported magnetic topological materials not sensitive to magnetic order, such as RMn_6Sn_6 (R = rare earth metal).[41–49] Therefore, unless otherwise emphasized, all ARPES spectra in this work are based on data measured at 14.7 K and the energy bands calculations are based on the nonmagnetic phase.

ARPES spectrum along high-symmetry paths is exhibited in Fig. 2(e), in comparison to the DFT projection results in Fig. 2(f). Around $\overline{\Gamma}$, ARPES measurements have found several hole-type bands which are centered at $\overline{\Gamma}$ and crossing Fermi level, forming closed hole pockets. Around $\overline{M}$, one electron type band is found to form the elliptical pocket. These bands can be well reproduced in the DFT calculation. By contrast, we find several pairs of bands at the $\overline{K}$ point and one shallow band at the $\overline{M}$ point (red arrows in Fig. 2(e)) residing in the bulk gap, which cannot be found in the DFT calculated bulk band spectra. This motivates us to attribute them to surface states and explore their termination origin in the following.

We employ termination-dependent band structure projections to illustrate the origin of these bands which are absent in the bulk calculation. Figures 3(a) and 3(b) show ARPES spectra along $\overline{\Gamma}$–$\overline{K}$–$\overline{M}$ taken with various photon energies. Potential surface state pairs at the $\overline{K}$ point are labeled as SS1–SS4 (red arrows). For different photon energies, while the intensity of these band pairs shows some variation, their energy location and band shape remain constant, suggesting a two dimensional behavior. For comparison, energy distribution curves (EDCs) at $\overline{K}$ are plotted to clarify the positions of the four sets of surface states at different photon energies. To shed light on the surface origin of these band pairs, DFT calculated band structures are projected onto (00l) surface with different terminating layers. As shown in Figs. 3(c) and 3(d), we treat all the atomic layers forming the repeating octuple layer as possible terminating layers (T1–T8) and present their corresponding projected surface and bulk spectra. In the energy window shown here, the surface band pairs show obvious termination dependence concerning the number of pairs and their location and dispersion. Basis similarity can be found between the ARPES measured surface spectra and the one calculated based on Au atomic layer termination (T1). All four sets of surface states are reproduced by the theoretical calculations. It is noted that some bands such as the bands with strong spectral weight right below SS4 and the deeper bands at about $E - E_F = -2.3$ eV in T1 panel are not observed experimentally, which may be due to the matrix element effect.

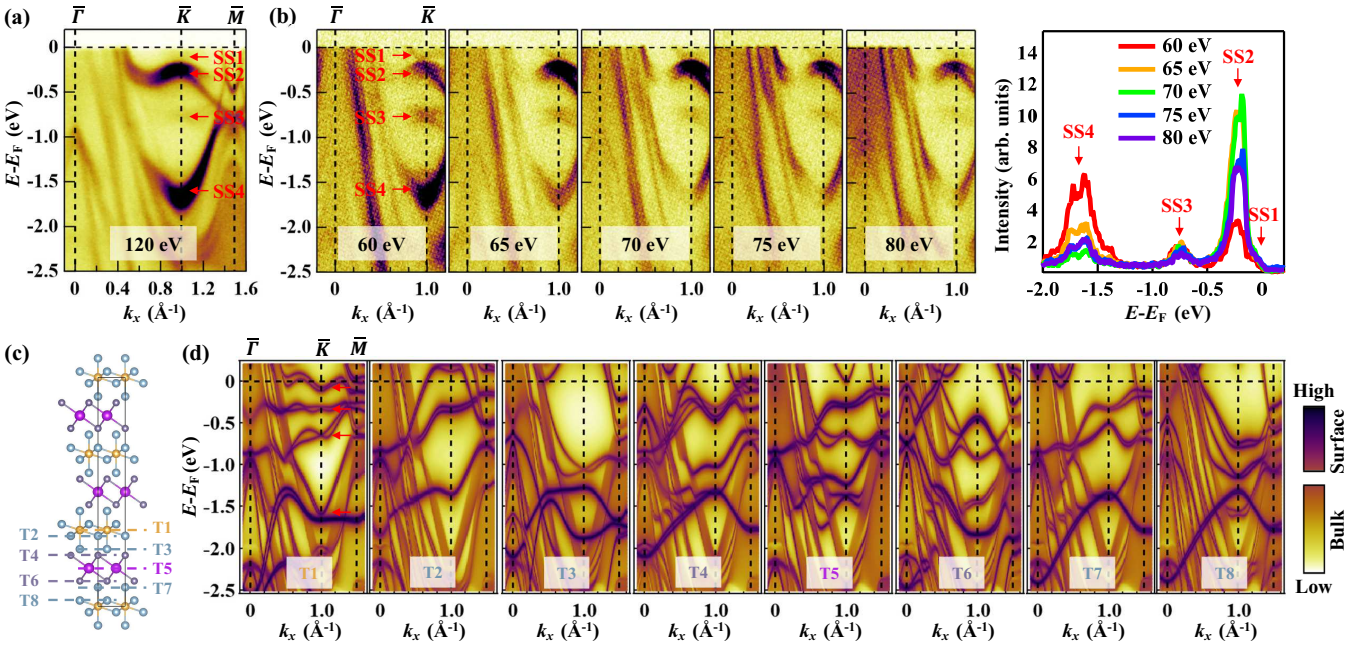


Fig. 3. Multiple surface states in $GdAuAl_4Ge_2$. (a) ARPES spectrum using incident photon energy of 120 eV along $\overline{\Gamma}$–$\overline{K}$–$\overline{M}$. The red arrows point to four sets of surface states at $\overline{K}$. (b) Same ARPES spectra but taken with various photon energies and corresponding EDCs at $\overline{K}$. (c) Crystal structure to illustrate the different cleavage planes for panel (d). The atomic layer crossed by each dashed line indicates the topmost atoms after cleavage. (d) Calculated surface states and bulk states projection onto (00l) surface with different terminating layers as shown in panel (c).

For band topology analysis, we perform parity calculations at the eight time-reversal invariant momenta (TRIM) to obtain the Z_2 topological invariant. As shown in Fig. 4(a), the bulk band structures are plotted along the high-symmetry k-paths. All the bands are two-fold degenerate due to the combined operation of time-reversal and inversion symmetries. The four bands highlighted by distinct colors near the fermi level are highly associated with the ARPES spectrums

discussed above. For the band indexes $n = 56$, 58, 60, 62, parity calculations run over all the n occupied bands, respectively. It is worth to note that the global band gap exists for all the selected occupied band numbers, making it possible to define the topological phases just as insulator systems. By taking the inversion symmetry into consideration, the Z_2 topological invariant is given by

$$(-1)^{\lambda} = \prod_{k_{\mathrm{TRIM}}, n\in \mathrm{occ}/2} \xi_n(k_{\mathrm{TRIM}}),$$

where k_{TRIM} are eight TRIM, ξ_n is the parity eigenvalue of the n-th band and λ is the strong Z_2 topological invariant. The results show that $GdAuAl_4Ge_2$ is a strong topological insulator with nontrivial surface states for the 56, 58, and 60 occupied bands. As for the 62 occupied band, $GdAuAl_4Ge_2$ is a weak topological insulator. To further examine the nontrivial topology, we also perform Wannier charge center calculations for the 60 occupied bands in the six key planes. As shown in Fig. 4(b), $Z_2 = 0$ is obtained in the three planes $k_x = 0/k_y = 0/k_z = 0$ and $Z_2 = 1$ is obtained in the three planes $k_x = \pi/k_y = \pi/k_z = \pi$, which are in good agreement with the results of parity calculations. To further elucidate the origin of topological band structures, we conduct an orbital analysis around the TRIM and obtain the projected band structures. The results demonstrate that band inversion occurs at multiple k-points, collectively leading to a nontrivial topology (see the detailed discussion in the supplementary material). In Figs. 4(c)–4(f), we plot the projected band structures for orbitals with dominant contributions near the Γ and F points as our examples. Band inversion features are clearly observed at both Γ and F points.

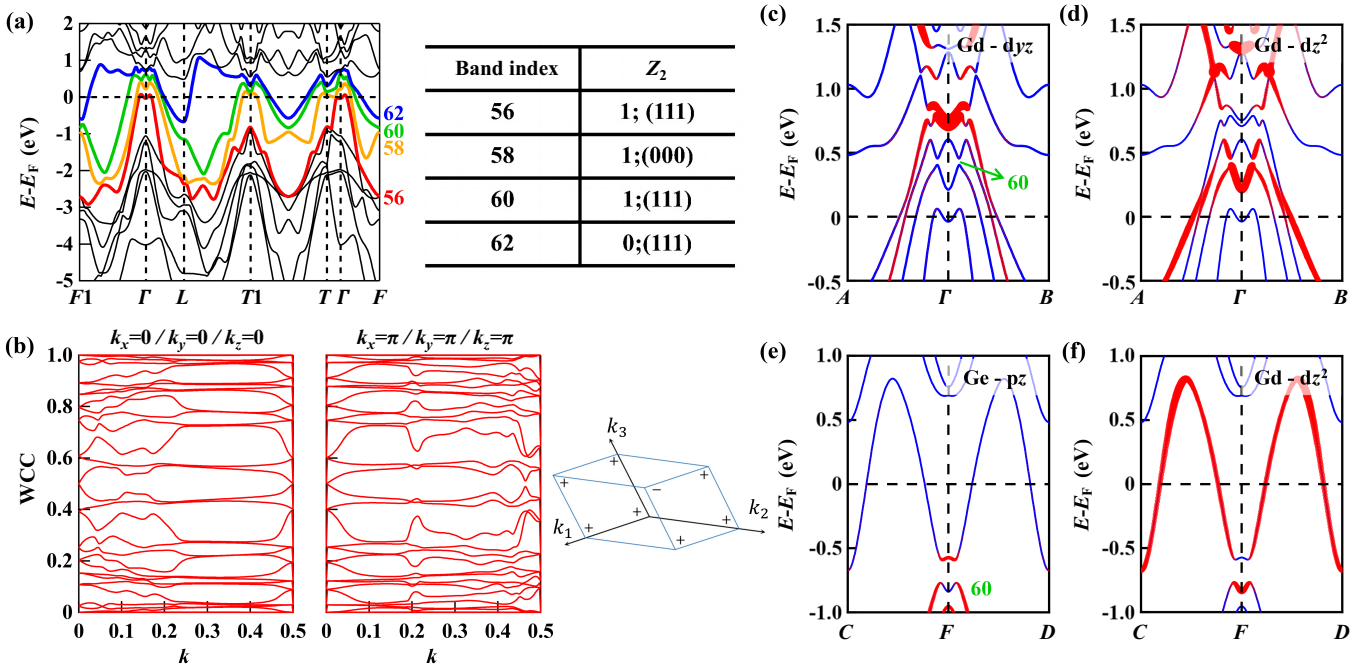


Fig. 4. Nontrivial Z_2 topology in $GdAuAl_4Ge_2$. (a) Band structures of $GdAuAl_4Ge_2$ and Z_2 topological invariants of specific band index. $\lambda;(\nu_1\nu_2\nu_3)$ includes one strong topological invariant λ and three weak topological invariants ν_i $(i = 1,2,3)$. Bold solid lines with distinct colors represent the n-th band ($n = 56$, 58, 60, 62). (b) The Wilson loop of $GdAuAl_4Ge_2$ for the band index 60, showing Wannier charge centers along specific k-path in the high-symmetry planes. (c)–(f) Projected band structures of specific orbitals near the time-reversal invariant momenta. The size of the red dots indicates the relative contribution weight of the associated orbitals. The coordinates of points A, B, C, and D are $\boldsymbol{k}_\Gamma - 0.5\boldsymbol{k}_1$, $\boldsymbol{k}_\Gamma + 0.5\boldsymbol{k}_1$, $\boldsymbol{k}_F - 0.5\boldsymbol{k}_3$, and $\boldsymbol{k}_F + 0.5\boldsymbol{k}_3$, respectively, where $\boldsymbol{k}_1$, $\boldsymbol{k}_2$, and $\boldsymbol{k}_3$ are the basis vectors of the reciprocal space.

4. Discussion

Combining experimental and calculational analyses, we have proved that there exists a strong topological insulator state in rare earth antiferromagnet $GdAuAl_4Ge_2$ with nontrivial surface states in its nonmagnetic phase. We have directly revealed multiple pairs of surface states whose topological nature remains to be clarified. In addition, while our first principles, parity, and Wilson loop calculations are all performed based on nonmagnetic phase, incorporating the antiferromagnetic order into calculation is highly desired to specify the magnetic topological phase. The magnetic fine structure of $GdAuAl_4Ge_2$ deserves further x-ray scattering study. Furthermore, Hall and Nernst measurements are needed to demonstrate its transport response steming from the interplay between magenetism and band topology.

Acknowledgments

Project supported by the National Key Research and Development Program of China (Grant No. 2022YFA1403700), the National Natural Science Foundation of China (Grant No. 12074163), the Basic and Applied Basic Research Foundation of Guangdong Province, China

(Grants Nos. 2022B1515020046, 2022B1515130005, and 2021B1515130007), the Innovative and Entrepreneurial Research Team Program of Guangdong Province, China (Grant Nos. 2019ZT08C044), and Shenzhen Science and Technology Program (Grant No. KQTD20190929173815000). C. C. acknowledges the assistance of SUSTech Core Research Facilities.

References

[1] Tokura Y, Yasuda K and Tsukazaki A 2019 *Nat. Rev. Phys.* **1** 126
[2] Bernevig B A, Felser C and Beidenkopf H 2022 *Nature* **603** 41
[3] Wang Y, Ma X M, Hao Z, Cai Y, Rong H, Zhang F, Chen W, Zhang C, Lin J, Zhao Y, Liu C, Liu Q and Chen C 2023 *Natl. Sci. Rev.* nwad066
[4] Wang Y, Zhang F, Zeng M, Sun H, Hao Z, Cai Y, Rong H, Zhang C, Liu C, Ma X, Wang L, Guo S, Lin J, Liu Q, Liu C and Chen C 2023 *Front. Phys.* **18** 21304
[5] Šmejkal L, MacDonald A H, Sinova J, Nakatsuji S and Jungwirth T 2022 *Nat. Rev. Mater.* **7** 482
[6] Tokura Y, Kawasaki M and Nagaosa N 2017 *Nat. Phys.* **13** 1056
[7] Armitage N P and Wu L 2019 *Scipost Phys.* **6** 046
[8] Fei F, Zhang S, Zhang M, Shah S A, Song F, Wang X and Wang B 2019 *Adv. Mater.* **32** e1904593
[9] Zhan G, Wang H and Zhang H 2020 *Physics* **49** 817 (in Chinese)
[10] He K 2020 *npj Quantum Mater.* **5** 90
[11] Ning W and Mao Z 2020 *APL Mater.* **8** 090701
[12] Li Y and Xu Y 2021 *Comput. Mater. Sci* **190** 110262
[13] Sekine A and Nomura K 2021 *J. Appl. Phys.* **129** 141101
[14] Sun H M and He Q L 2021 *Acta Phys. Sin.* **70** 127302 (in Chinese)
[15] Wang P, Ge J, Li J, Liu Y, Xu Y and Wang J 2021 *Innovation* **2** 100098
[16] Zhao Y and Liu Q 2021 *Appl. Phys. Lett.* **119** 060502
[17] Armitage N P, Mele E J and Vishwanath A 2018 *Rev. Mod. Phys.* **90** 015001
[18] Liu E and Zhang S 2019 *Sci. Sin.-Phys. Mech. As.* **49** 127001
[19] Otrokov M M, Klimovskikh, II, Bentmann H, *et al.* 2019 *Nature* **576** 416
[20] Gong Y, Guo J, Li J, *et al.* 2019 *Chin. Phys. Lett.* **36** 076801
[21] Li J, Li Y, Du S, Wang Z, Gu B L, Zhang S C, He K, Duan W and Xu Y 2019 *Sci. Adv.* **5** eaaw5685
[22] Otrokov M M, Rusinov I P, Blanco-Rey M, Hoffmann M, Vyazovskaya A Y, Eremeev S V, Ernst A, Echenique P M, Arnau A and Chulkov E V 2019 *Phys. Rev. Lett.* **122** 107202
[23] Sun H, Xia B, Chen Z, Zhang Y, Liu P, Yao Q, Tang H, Zhao Y, Xu H and Liu Q 2019 *Phys. Rev. Lett.* **123** 096401
[24] Zhang D, Shi M, Zhu T, Xing D, Zhang H and Wang J 2019 *Phys. Rev. Lett.* **122** 206401
[25] Chen Y J, Xu L X, Li J H, *et al.* 2019 *Phys. Rev. X* **9** 041040
[26] Lu R, Sun H, Kumar S, *et al.* 2021 *Phys. Rev. X* **11** 011039
[27] Gao A, Liu Y F, Hu C, *et al.* 2021 *Nature* **595** 521
[28] Deng Y, Yu Y, Shi M Z, Guo Z, Xu Z, Wang J, Chen X H and Zhang Y 2020 *Science* **367** 895
[29] Ge J, Liu Y, Li J, Li H, Luo T, Wu Y, Xu Y and Wang J 2020 *Natl. Sci. Rev.* **7** 1280
[30] Liu C, Wang Y, Li H, Wu Y, Li Y, Li J, He K, Xu Y, Zhang J and Wang Y 2020 *Nat. Mater.* **19** 522
[31] Liu C, Wang Y, Yang M, Mao J, Li H, Li Y, Li J, Zhu H, Wang J, Li L, Wu Y, Xu Y, Zhang J and Wang Y 2021 *Nat. Commun.* **12** 4647
[32] Kang M, Ye L, Fang S, *et al.* 2020 *Nat. Mater.* **19** 163
[33] Ye L, Kang M, Liu J, von Cube F, Wicker C R, Suzuki T, Jozwiak C, Bostwick A, Rotenberg E, Bell D C, Fu L, Comin R and Checkelsky J G 2018 *Nature* **555** 638
[34] Kuroda K, Tomita T, Suzuki M T, *et al.* 2017 *Nat. Mater.* **16** 1090
[35] Nakatsuji S, Kiyohara N and Higo T 2015 *Nature* **527** 212
[36] Reichlova H, Janda T, Godinho J, Markou A, Kriegner D, Schlitz R, Zelezny J, Soban Z, Bejarano M, Schultheiss H, Nemec P, Jungwirth T, Felser C, Wunderlich J and Goennenwein S T B 2019 *Nat. Commun.* **10** 5459
[37] Liu D F, Liang A J, Liu E K, Xu Q N, Li Y W, Chen C, Pei D, Shi W J, Mo S K, Dudin P, Kim T, Cacho C, Li G, Sun Y, Yang L X, Liu Z K, Parkin S S P, Felser C and Chen Y L 2019 *Science* **365** 1282
[38] Liu E, Sun Y, Kumar N, *et al.* 2018 *Nat. Phys.* **14** 1125
[39] Belopolski I, Chang G, Cochran T A, *et al.* 2022 *Nature* **604** 647
[40] Chang G, Xu S Y, Zhou X, Huang S M, Singh B, Wang B, Belopolski I, Yin J, Zhang S, Bansil A, Lin H and Hasan M Z 2017 *Phys. Rev. Lett.* **119** 156401
[41] Ghimire N J, Dally R L, Poudel L, Jones D C, Michel D, Magar N T, Bleuel M, McGuire M A, Jiang J S, Mitchell J F, Lynn J W and Mazin I I 2020 *Sci. Adv.* **6** eabe2680
[42] Yin J X, Ma W, Cochran T A, *et al.* 2020 *Nature* **583** 533
[43] Dhakal G, Cheenicode Kabeer F, Pathak A K, Kabir F, Poudel N, Filippone R, Casey J, Pradhan Sakhya A, Regmi S, Sims C, Dimitri K, Manfrinetti P, Gofryk K, Oppeneer P M and Neupane M 2021 *Phys. Rev. B* **104** L161115
[44] Li M, Wang Q, Wang G, Yuan Z, Song W, Lou R, Liu Z, Huang Y, Liu Z, Lei H, Yin Z and Wang S 2021 *Nat. Commun.* **12** 3129
[45] Ma W, Xu X, Yin J X, Yang H, Zhou H, Cheng Z J, Huang Y, Qu Z, Wang F, Hasan M Z and Jia S 2021 *Phys. Rev. Lett.* **126** 246602
[46] Peng S, Han Y, Pokharel G, Shen J, Li Z, Hashimoto M, Lu D, Ortiz B R, Luo Y, Li H, Guo M, Wang B, Cui S, Sun Z, Qiao Z, Wilson S D and He J 2021 *Phys. Rev. Lett.* **127** 266401
[47] Gu X, Chen C, Wei W S, *et al.* 2022 *Phys. Rev. B* **105** 155108
[48] Hu Y, Wu X, Yang Y, Gao S, Plumb N C, Schnyder A P, Xie W, Ma J and Shi M 2022 *Sci. Adv.* **8** eadd2024
[49] Yang T Y, Wan Q, Song J P, Du Z, Tang J, Wang Z W, Plumb N C, Radovic M, Wang G W, Wang G Y, Sun Z, Yin J X, Chen Z H, Huang Y B, Yu R, Shi M, Xiong Y M and Xu N 2022 *Quantum Frontiers* **1** 14
[50] Wu X and Kanatzidis M G 2005 *J. Solid State Chem.* **178** 3233
[51] Feng K, Leahy I A, Oladehin O, Wei K, Lee M and Baumbach R 2022 *J. Magn. Magn. Mater.* **564** 170006
[52] Canfield P C, Kong T, Kaluarachchi U S and Jo N H 2016 *Philos. Mag.* **96** 84
[53] Hohenberg P and Kohn W 1964 *Phys. Rev.* **136** B864
[54] Kohn W and Sham L J 1965 *Phys. Rev.* **140** A1133
[55] Kresse G and Furthmüller J 1996 *Phys. Rev. B* **54** 11169
[56] Monkhorst H J and Pack J D 1976 *Phys. Rev. B* **13** 5188
[57] Liechtenstein A I, Anisimov V I and Zaanen J 1995 *Phys. Rev. B* **52** R5467
[58] Mostofi A A, Yates J R, Lee Y S, Souza I, Vanderbilt D and Marzari N 2008 *Comput. Phys. Commun.* **178** 685
[59] Marzari N, Mostofi A A, Yates J R, Souza I and Vanderbilt D 2012 *Rev. Mod. Phys.* **84** 1419